

**Photon detection inefficiency
measurements using tagged photons from
the decay $K^+ \rightarrow \pi^+ \pi^0$
(master thesis)**

February 6 1997

Takafumi Sasaki

Department of Physics, Osaka University

Abstract

The E787 group searches for the $K^+ \rightarrow \pi^+ \nu \bar{\nu}$ decay at the Brookhaven National Laboratory. One of the main backgrounds is $K^+ \rightarrow \pi^+ \pi^0$. Therefore the π^0 rejection is crucial for this study. For future upgrades of the photon detector, we plan to understand the π^0 detection inefficiency in terms of the single photon detection inefficiency.

By using tagged photons from the $K^+ \rightarrow \pi^+ \pi^0$ decays, we measured the photon detection inefficiency of the E787 detector as a function of the missing photon's energy and the direction, which were determined by fitting kinematic variables of the π^+ and the observed photon.

A detection inefficiency of π^0 is estimated as a product of a pair of single gamma detection inefficiencies. By examining a threshold energy dependence of the π^0 detection inefficiency, a new source of a π^0 missing mechanism is identified.

A possible improvement of the photon detection system is discussed. And a future prospect of lowering the upper limit for $\pi^0 \rightarrow \nu \bar{\nu}$ is given.

Contents

1	Introduction	3
1.1	The $K^+ \rightarrow \pi^+ \nu \bar{\nu}$ experiment	3
1.2	Measuring the photon detection inefficiency	4
1.3	Barrel Veto Liner	5
1.4	The $\pi^0 \rightarrow \nu \bar{\nu}$ decay	5
2	Apparatus	6
2.1	LESB-III beam line	6
2.2	The detector	6
2.2.1	Beam counter	7
2.2.2	Target	7
2.2.3	Ultra Thin Chamber(UTC)	7
2.2.4	Range Stack(RS)	7
2.2.5	Barrel Veto counter(BV)	8
2.2.6	End Cap photon veto counter(EC)	8
3	Online event selection	11
4	Offline event selection	13
4.1	Pass1	13
4.1.1	UTC and RS tracking	13
4.1.2	TARGET and IC reconstruction	14
4.1.3	total momentum, range cut	14
4.1.4	1GAMMA	14
4.1.5	intime photon veto cuts	14
4.2	Selection of missing γ events	15
5	Inefficiency	21
5.1	Single photon detection inefficiency	21
5.2	π^0 detection inefficiency	23
6	Barrel Veto Liner	36
7	Conclusion	37

List of Figures

1.1	The first order process	3
1.2	The second order process	4
2.1	The LESB-III beam line	9
2.2	The overview of the E787 detector	10
3.1	The momentum spectra for top 6 K^+ decay modes	12
4.1	E_{meas} vs. E_{true}	17
4.2	E_{fit} vs. E_{true}	17
4.3	ϕ_{fit} vs. ϕ_{true}	18
4.4	$\sin \theta_{fit}$ vs. $\sin \theta_{true}$	18
4.5	$\sin(\theta_{fit})$, $E_{fit} > 123 \text{ MeV}$	19
4.6	$\sin(\theta_{fit})$, $E_{fit} < 123 \text{ MeV}$	19
5.1	The way that the two photons hit the same segment.	24
5.2	$\cos(\phi_{\gamma 1} - \phi_{\gamma 2})$ (E in BV $> 5 \text{ MeV}$)	25
5.3	$\cos(\phi_{\gamma 1} - \phi_{\gamma 2})$ (E in BV $< 5 \text{ MeV}$)	25

Chapter 1

Introduction

1.1 The $K^+ \rightarrow \pi^+ \nu \bar{\nu}$ experiment

The E787 group is running at the Low Energy Separated Beam(LESB-III) line at the Alternating Gradient Synchrotron (AGS) in Brookhaven National Laboratory. The goal is a measurement of the branching ratio of the K^+ rare decay $K^+ \rightarrow \pi^+ \nu \bar{\nu}$ since 1988.

The $K^+ \rightarrow \pi^+ \nu \bar{\nu}$ decay, a Flavor Changing Neutral Current, is forbidden at the first order(Figure 1.1).

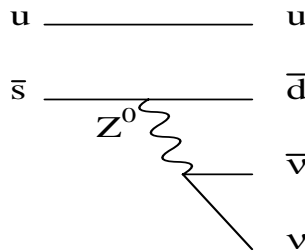


Figure 1.1: The first order process

At the second order, the decay is allowed via two “penguin” and one box diagram (Figure 1.2).

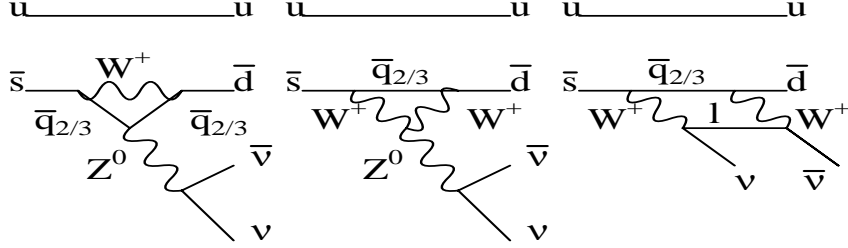


Figure 1.2: The second order process

The top quark contribution to the $K^+ \rightarrow \pi^+ \nu \bar{\nu}$ branching ratio for three ν generations is

$$\begin{aligned} \frac{B(K^+ \rightarrow \pi^+ \nu \bar{\nu})}{B(K^+ \rightarrow \pi^0 e^+ \nu_e)} &= \frac{3}{2} \left(\frac{\alpha}{\pi \sin^2 \theta_W} \right)^2 \frac{|V_{ts}^* V_{td}|^2}{|V_{td}|^2} [X(x_t)]^2 \\ &= \frac{3}{2} \left(\frac{\alpha}{\pi \sin^2 \theta_W} \right)^2 A^4 \lambda^8 [(1 - \rho)^2 + \eta^2] [X(x_t)]^2 \end{aligned}$$

where V_{xx} is the Cabbibo-Kobayashi-Maskawa matrix(V_{CKM}), A, λ, η and ρ are the Wolfenstein V_{CKM} parameters, and

$$X(x_t) = \frac{x_t}{8} \left(\frac{x_t + 2}{x_t - 1} + \frac{3x_t - 6}{(x_t - 1)^2} \ln x_t \right) \simeq 0.65 x_t^{0.59}$$

with $x_t = m_t^2/m_W^2$

Substituting $\lambda = 0.22$, $\alpha = 1/128$, $\sin^2 \theta_W = 0.23$, $B(K^+ \rightarrow \pi^0 e^+ \nu_e) = 0.0482$, $X(x_t) \simeq 0.65 x_t^{0.59}$, and including the charm contribution yields

$$B(K^+ \rightarrow \pi^+ \nu \bar{\nu}) \simeq 1.97 \times 10^{-11} A^4 x_t^{1.18} [(\rho_0 - \rho)^2 + \eta^2]$$

Considering all uncertainties, $B(K^+ \rightarrow \pi^+ \nu \bar{\nu})$ will be within $(0.3-3) \times 10^{-10}$ [3].

The present experimental upper limit is 2.4×10^{-9} (90% C.L.) , which was obtained by analyzing 1989-1991 data[4].

1.2 Measuring the photon detection inefficiency

In the $K^+ \rightarrow \pi^+ \nu \bar{\nu}$ study, one of the main backgrounds is $K^+ \rightarrow \pi^+ \pi^0$. If the π^0 is not detected for some reason and kinematic variables of the π^+ are miss-measured, the

decay looks like $K^+ \rightarrow \pi^+ \nu \bar{\nu}$. Therefore rejecting π^0 is crucial for the experiment. In this study a π^0 detection inefficiency was calculated as a product of the single photon detection inefficiencies.

First we required the charged particle to be the π^+ from the $K^+ \rightarrow \pi^+ \pi^0$ decay. Since $K^+ \rightarrow \pi^+ \pi^0$ is a two body decay, the momentum and energy distributions of the particles have monochromatic peaks. Second we required one photon detected in the detector called Barrel Veto counter (BV) and no the other photon anywhere. And then, using the kinematic variables of the tagged photon and the π^+ , we determined the energy and the direction of the undetected photon. For the denominators, a sample without online-offline photon vetoes was used.

1.3 Barrel Veto Liner

Although the detector in E787 is almost a 4π photon detector, the total radiation length is not enough for the 45 degree direction from the center of the detector with respect to the beam direction[5]. In order to improve the sensitivity for the $K^+ \rightarrow \pi^+ \nu \bar{\nu}$ for the future runs, a new detector called Barrel Veto Liner is planned to install. We estimated how much the new detector would improve the π^0 detection efficiency.

1.4 The $\pi^0 \rightarrow \nu \bar{\nu}$ decay

The decay $\pi^0 \rightarrow \nu \bar{\nu}$ is suppressed if the neutrino has purely left handed helicity. But if the neutrino mass is not zero and the Z^0 couples to the right handed neutrino with the standard weak interaction strength, the branching ratio has a maximum value of 3×10^{-9} . The current upper limit of 8.3×10^{-7} was obtained by analyzing E787 data[6]. In their analysis, the π^0 detection inefficiency was considered as the systematic error. So our result of the inefficiency would improve the limit.

Chapter 2

Apparatus

2.1 LESB-III beam line

The overview of the detector is shown in Fig2.1. After the 24GeV protons from the BNL Alternating Gradient Synchrotron(AGS) hit the 6cm platinum, the water cooled production target, K s, π s and other particles are produced. By using two DC separators in the upstream of the detector, K/π ratio becomes about three. The 800MeV/c K^+ beam intensity is $\sim 7 \times 10^6/spill$.

2.2 The detector

The K^+ stops and decays in the target. When the decay $K^+ \rightarrow \pi^+ \nu \bar{\nu}$ occurs, the detectable particle produced in the decay is only one π^+ . The detector has powerful 4π γ veto system described later. The momentum, the energy and the range of the charged decay particle are measured by drift chambers and range counters located around the target.

The overview of the detector is shown in Fig2.2.

2.2.1 Beam counter

At first the incoming K^+ from AGS passes a Čerenkov Counter. The Čerenkov Counter is used for the K^+ tagging which is used as a trigger(\check{C}_K) and the offline analysis. The counter is also used for the π^+ tagging(\check{C}_π).

The 3 plane beam wire chambers are put at the downstream of the Čerenkov Counter. The chambers ensure that only one K^+ enters the detector and no extra K^+ or π^+ is present at the apparent K^+ decay time.

The BeO and the Pb-Glass degraders are located at the downstream of the beam wire chambers. The lead-glass degrader for the passing K^+ detects Čerenkov light from the passing K^+ .

The K^+ passes through the degrader, a two-plane hodoscope(the B4 counter), the parallel fingers of scintillator read out by phototubes. These hodoscopes identify the π and the μ by using the minimum ionizations.

2.2.2 Target

The K^+ stopping target consists of $5mm \times 5mm$ 413 plastic scintillation fibers and many small fibers in order to measure the K^+ stopping position. The length of each fiber is 20.0cm. The signals from them are read out by PMT located outside of the magnetic field at the downstream end of the detector. The incoming K^+ stops after exciting ~ 5 fibers, and decays. Almost all charged particles among decay products(π, μ) go out of the target after exciting $5 \sim 10$ fibers with minimum ionizing. Then fired fibers are identified as K^+ 's cells or charged decay products($\pi^+, \mu^+ \dots$) cells by the energy deposit in it and hit timing. Typically, the energy deposit of a fiber fired by the stopping K^+ is $\geq 3MeV$ and ones by the charged decay particle is $\leq 2MeV$. The 6 plastic scintillation counters called I-counter(IC) are located around this target in order to help to distinguish hits in the fiducial region.

2.2.3 Ultra Thin Chamber(UTC)

The cylindrical drift chamber surrounds the target in order to measure the momentum of the decay particles. The drift chamber system is composed of three super layers. The inner radius is 8.0 cm and the outer radius is 42.8 cm. It subtends a solid angle of about $2\pi st$. The half-width of a square cell is $5 \sim 9mm$ which is dependent on the super layer. The number of total channels is 3600, 1152×2 (ADC and TDC) anode channels and 768×2 cathode channel. The chamber is operated with 50-50 mixture gas of $Ar H_2C_6$ and bubbled Ethanol. The node wire were supplied High Voltage $+1850 \sim +2000V$. The resolution of the space was about $120\mu m, 300\mu m, 250 \sim 400\mu m$ in the middle of the cell, near the anode wire and near the corner, respectively.

2.2.4 Range Stack(RS)

The cylindrical Range counter called Range Stack, which consists of the 21 plastic scintillator layers segmented into 24 sectors are located the outside of UTC. The signal from PMT on the Range Stack are recorded by 50MHz Transient Digitizer(TD). The

Range Stack detects the decay sequence of the charged particles(for example, $\pi \rightarrow \mu \rightarrow e$) and measures the energy deposit and the range of it in the Range Stack. Two proportional chambers are sets in the Range Stack in order to measure the Z positions of the track and refine the range resolution.

2.2.5 Barrel Veto counter(BV)

The Barrel Veto counter is located around the Range Stack counter. It consists of alternating layers of the 1.0 mm thick lead and the 5.0mm thick plastic scintillator. The Barrel Veto is segmented into 48 azimuthal sectors with each sectors further segmented into 4 radial layers. The active region of the Barrel Veto is 1.9m long and covered about two-thirds solid angle corresponding to the 90 degree of the solid angle. Its thickness corresponds to 14.3 radiation lengths. The signals from each modules are read by phototubes located outside the magnet endplate. The Barrel Veto counter is used as the online and offline photon veto system for searching the $K^+ \rightarrow \pi^+ \nu \bar{\nu}$ signal. We used this system as the photon counter for the detection of $K^+ \rightarrow \pi^+ \pi^0, \pi^0 \rightarrow \gamma \gamma$ signals.

2.2.6 End Cap photon veto counter(EC)

The EndCap photon Veto counters cover the region upstream and downstream of UTC. The upstream EndCap is segmented into 75 and the downstream one is 68. Each modules are composed of pure CsI crystals and fine-mesh phototubes attached directly to the crystals. The signals from each modules are read by ADC, TDC and CCD transient Digitizer in order to record the CsI output pulse shape for the improvement of the timing resolution of the low energy photon and the reduction of the accidental veto in the high rate environment.

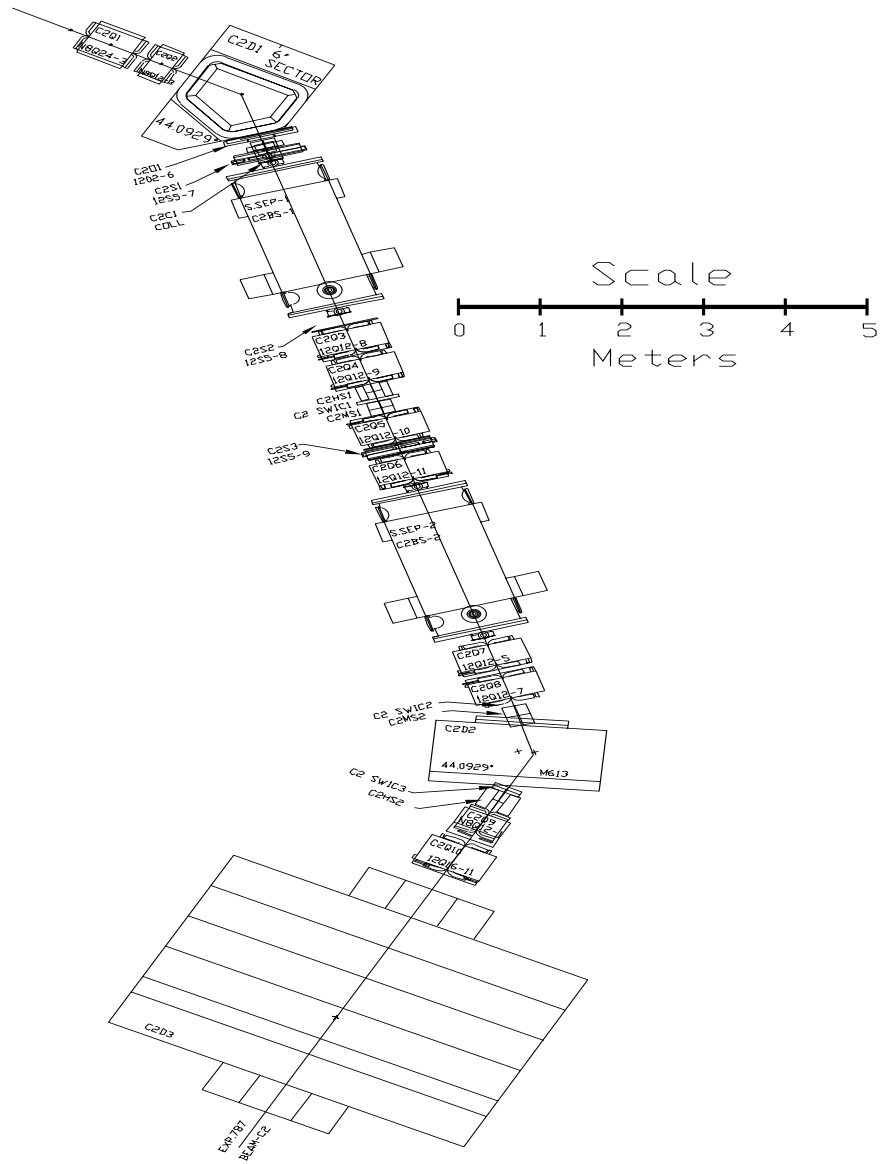


Figure 2.1: The overview of the BNL LESB-III beam line

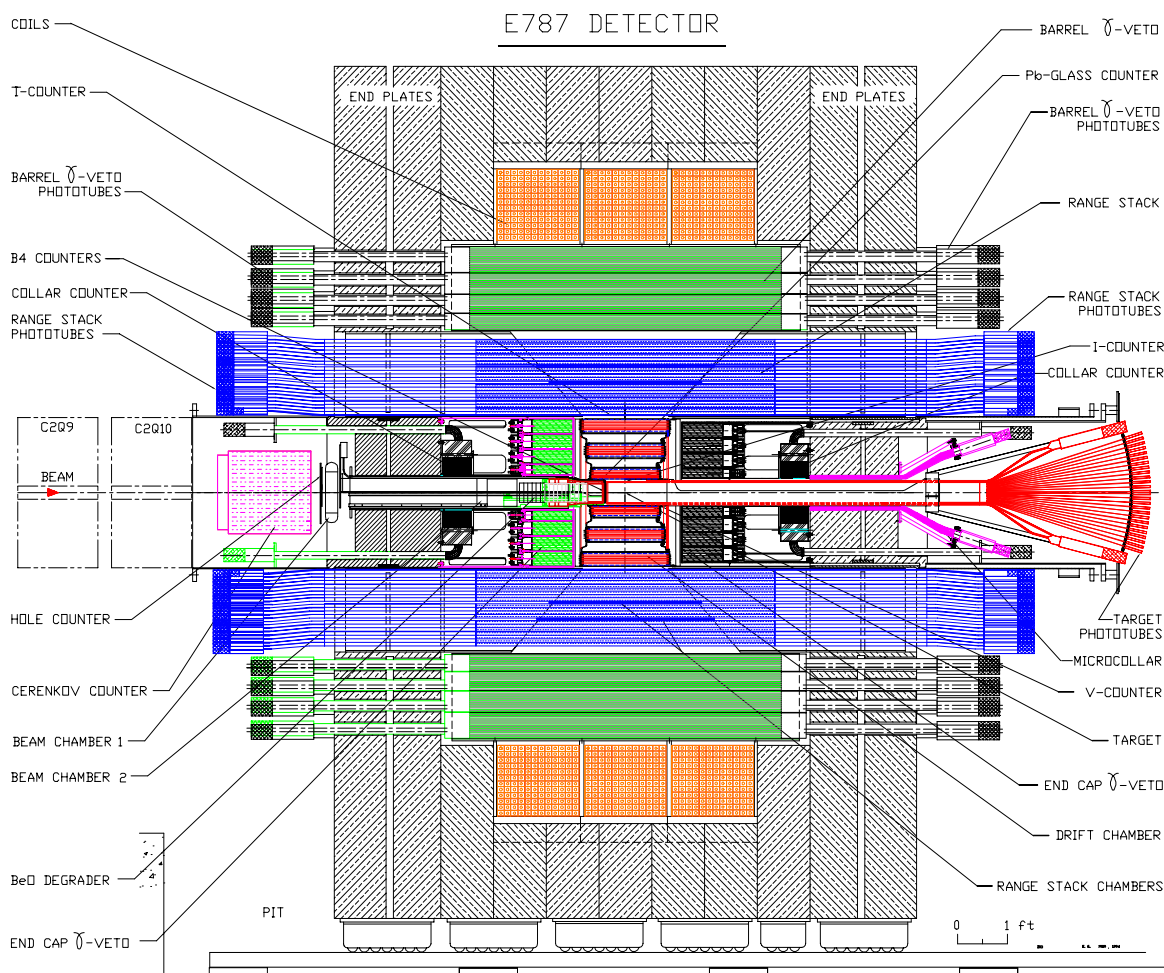


Figure 2.2: The overview of the E787 detector

Chapter 3

Online event selection

In our experiment, the triggers were determined by the electronics called trigger board. It calculated the trigger bit using the discriminated PMT signals from various detector elements. In order to check the detector performance, our experiment took some monitor data (for example, triggered for $K^+ \rightarrow \pi^+\pi^0$ and $K^+ \rightarrow \mu^+\nu$) as well as $K^+ \rightarrow \pi^+\nu\bar{\nu}$ triggered data. Events which passed one of the trigger were written to magnetic tapes. In 1996, E787 group installed the special online trigger called 1γ trigger in order to detect such events; π^0 from $K^+ \rightarrow \pi^+\pi^0$ decays into 2γ , only one of the 2γ is detected in BV, and another γ is not detected anywhere.

The 1γ trigger logic was defined as;

$$KB \cdot IC \cdot DC \cdot T.2 \cdot (6ct + 7ct) \cdot \overline{(19ct + 20ct + 21ct)} \cdot \overline{EC} \cdot HEXCUT \cdot NG1 \cdot L1.1$$

where

1. KB: A K^+ from the beam enters the target ($\check{C}_K \cdot B4 \cdot E_{TG}$)
2. IC: The I-counter hit
3. DC: The delayed coincidence between IC and \check{C}_K in order to reject scatter π^+ events
4. T.2: The trigger counter hit, which is the bottom layer of Range Stuck
5. $Xct + Yct + \dots$: Xth., Yth, \dots The layers in Range Stack hit within the gated time
6. EC: The End Cap γ hit
7. HEXCUT: There is only one hextant of Range Stack in which the energy deposit is greater than 10MeV.
8. NG1: The number of photon clusters in the Barrel Veto counter is less than 2
9. L1.1: TD area vs. height cut; select π^+

We got about 10^6 K^+ decay signals by the 1γ trigger through 1996 run.

K^+ decay mode	Branching ratio
$\mu^+ \nu_\mu$	0.635($K_{\mu 2}$)
$\pi^+ \pi^0$	0.216($K_{\pi 2}$)
$\pi^+ \pi^+ \pi^-$	0.056
$\pi^0 e^+ \nu_e$	0.048($K_{e 3}$)
$\pi^0 \mu^+ \nu_\mu$	0.032($K_{\mu 3}$)
$\pi^+ \pi^0 \pi_0$	0.017

Table 3.1: The branching ratio of top 6 K^+ decay modes

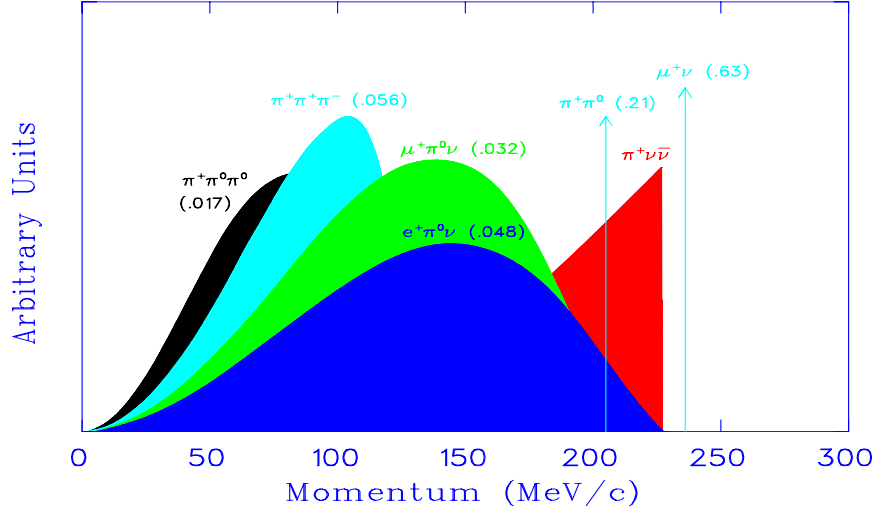


Figure 3.1: momentum spectrum of charged decay particle for top 6 K^+ decay mode

Chapter 4

Offline event selection

4.1 Pass1

Cuts	Examined	Passed	Failed	Rejection
TRKTIM	897809	888889	8920	1.01004
UTCTRAK	888889	868646	20243	1.02330
RDTRAK	868646	866201	2445	1.00282
TARGET	866201	840603	25598	1.03045
ICOUNTER	840603	835925	4678	1.00560
PTOTAL	835925	761346	74579	1.09796
RTOTAL	761346	717675	43671	1.06085
1GAMMA	717675	717291	384	1.00054
BVINTIME	717291	677807	39484	1.05825
ECINTIME	677807	520770	157037	1.30155
RSINTIME	520770	327700	193070	1.58917
ICINTIME	327700	294356	33344	1.11328
VCINTIME	294356	289389	4967	1.01716

Table 4.1: Summary of Pass1 analysis

In order to reduce the data size without losing the acceptance of the 1γ events, we divided the offline analysis into 2 stages. At the first step of our analysis, successful reconstructions of π^+ variables were required. Loose photon veto cuts were applied to reduce the total number of events. Much tighter photon vetoes were applied in the next stage. The summary of the Pass1 analysis was shown in the table(4.1).

4.1.1 UTC and RS tracking

TRKTIM required the Range Stack timing was found. **UTCTRACK** required the number of chamber(UTC) tracks was greater than 0. The Range Stack tracking used the TD information to find continuous hits in each layers in the same TD based timing

region. **RDTRK** checked whether a (or more than one) track(s) in Range Stack was reconstructed.

4.1.2 TARGET and IC reconstruction

TARGET and **ICOUNTER** required the target/IC reconstruction was O.K.

4.1.3 total momentum, range cut

To select $K^+ \rightarrow \pi^+\pi^0$ events, the events for which

$$196MeV/c \leq P_{total} \leq 230MeV/c$$

and

$$26.7cm \leq R_{total} \leq 34.8cm$$

were kept. The cut were called **PTOTAL** and **RTOTAL**, respectively.

4.1.4 1GAMMA

We reconstructed the γ cluster connected hit region in Barrel Veto counter. **1GAMMA** required a γ cluster in Barrel Veto counter in offline.

4.1.5 intime photon veto cuts

Photon vetoes were applied using so called the 'intime' routine. **BVINTIME**, **ECINTIME**, **RSINTIME**, **ICINTIME** and **VCINTIME** mean the photon vetoes for the subsystems of BV, EC, RS, IC and VC, respectively. Before applying **BVINTIME**, a clustering was performed by finding connected regions of BV hit elements. **BVINTIME** was applied against the sum of the energies of the second largest cluster and the smaller ones.

The time windows and the energy thresholds are listed in the Table(4.2).

System	time offset(nsec)	time window (nsec)	energy threshold (MeV)
BV	0.0	2.0	5.0
EC	0.0	2.0	10.0
RS	0.0	1.5	3.0
IC	0.0	2.0	4.0
VC	0.0	1.0	4.0

Table 4.2: A list of photon veto cuts used in Pass1

4.2 Selection of missing γ events

In the next step, tighter energy-momentum-range cuts were applied together with a dip angle cut in order to purify the sample further. Tight photon vetoes were also applied. Again the energy of the largest photon cluster in BV was excluded prior to the BV cut.

System	time offset(nsec)	time window(nsec)	energy threshold(MeV)
BV	4.0	7.5	0.4
EC	0.5	2.5	2.0
RS	4.0	5.5	2.0
TG	-0.5	2.0	1.5
IC	-0.5	3.5	2.5
VC	-4.5	5.5	1.5
CO	0.0	2.0	2.0
CM	0.0	2.0	2.0
EU	0.5	2.0	1.5

Table 4.3: A list of photon veto cuts used in Pass2

For the remaining events, a 3-constrained kinematic fit was carried out to minimize a χ^2 defined by

$$\chi^2 = \sum \left(\frac{X_{mes.}^i - X_{fit.}^i}{\sigma_{mes.}} \right)^2 \quad (4.1)$$

where $X_{mes.}^i$'s were 7 measured variables listed in the table 4.4.

The 3 constrains were the π^0 mass shell condition, the π^+ mass shell condition and the total energy conservation.

$$2E_{\gamma_1} E_{\gamma_2} (1 - \cos(\phi_{\gamma_1 \gamma_2})) = m_{\pi^0}^2$$

$$\frac{P_{\pi}^2 - T_{\pi}^2}{2T_{\pi}^2} = m_{\pi^+}$$

$$E_{\pi^+} + m_{\pi^+} + E_{\gamma_1} + E_{\gamma_2} = m_{K^+}$$

The errors used were listed also in the table 4.4.

To check the fitting, K_{π^2} events in Monte Carlo simulation were analyzed. Figure(4.1) is a scatter plot of the measured photon's energy versus true one. The vertical axis is a measured one. Figure(4.2) is a scatter plot of the fitted photon's energy versus true one. The vertical axis is a fitted one. Figure(4.3) is a scatter plot of the fitted photon's ϕ direction versus true one. Figure(4.4) is the one as to $\sin \theta$. Those figures show the fitting works well.

Figure(4.5) and Figure(4.6) are the θ -distributions of the high energy missing γ and the low energy missing γ in the real 1 γ data, respectively.

Variable	Definition	error
E_{π^+}	energy of a π^+	3.69
P_{π^+}	momentum of a π^+	2.67
θ_{π^+}	dip angle of a π^+	$0.04 \times \cos^2 \theta_{\pi^+}$
ϕ_{π^+}	azimuthal angle of a π^+	0.03
E_γ	energy of a γ	$1.834 \times \sqrt{E_\gamma}$
θ_γ	dip angle of a γ	$0.075 \times \cos^2 \theta_\gamma$
ϕ_γ	azimuthal angle of a γ	0.045

Table 4.4: 7 kinematic variables

The summary of the Pass2 analysis is shown in the table(4.5). Where, xxPV means a photon veto cut in the detector xx. Cut parameters are shown in the table4.3. PTOTAL, ETOTAL and RTOTAL requires $196.5 < P_{total} < 214.1$, $96.6 < E_{total} < 120.3$ and $26.9 < R_{total} < 34.6$, respectively. (E_{total} is a total energy of the charged particle.) PBPV requires the number of hits in the lead glass counter is less than 2. TZMAX requires the maximum Z difference of the hits within the photon cluster in BV is less than 112.5 cm. This cut will exclude the events in which two photons hit the same segment of BV and look like one photon. WSTP requires $-0.45 < \sin \theta_{\pi^+} < 0.45$. This will cut the asymmetrical tail of θ_{π^+} distribution. FIT requires the fitting is successful. PROB requires the χ^2 probability $\text{Prob}(\chi^2) > 0.2$. This cut will reduce the event which is not K_{π^2} or the event in which the kinematic variables are not measured correctly.

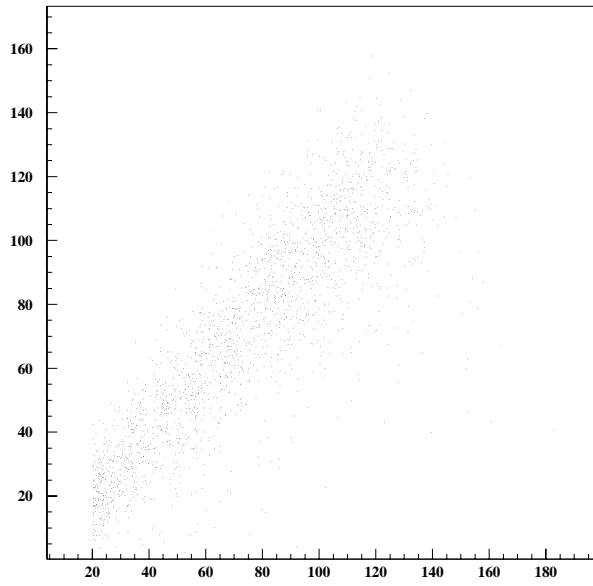


Figure 4.1: E_{meas} vs. E_{true}

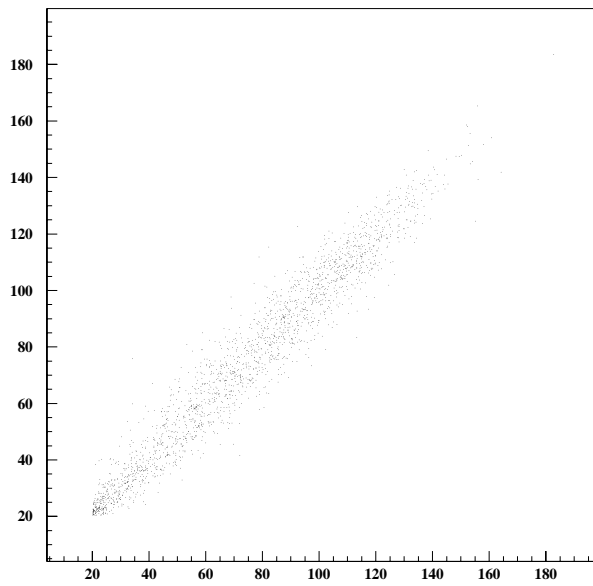


Figure 4.2: E_{fit} vs. E_{true}

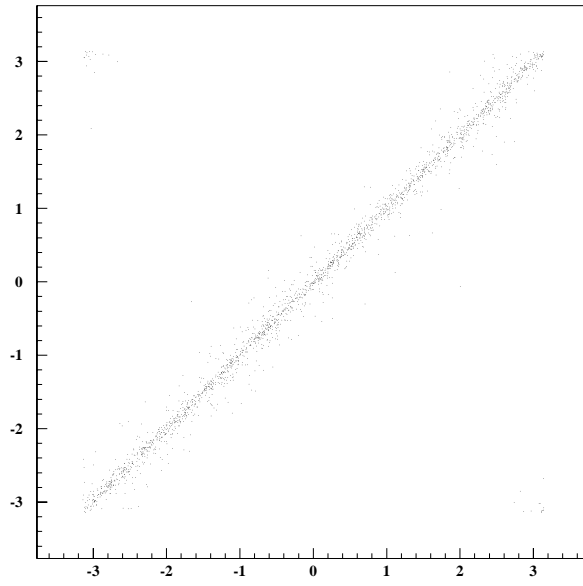


Figure 4.3: ϕ_{fit} vs. ϕ_{true}

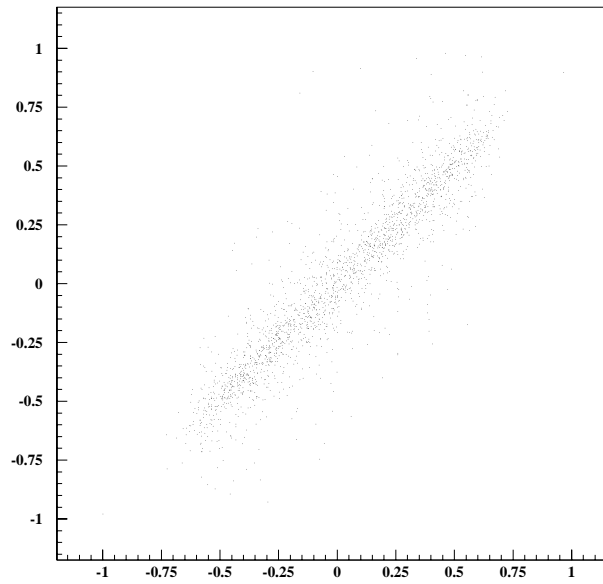
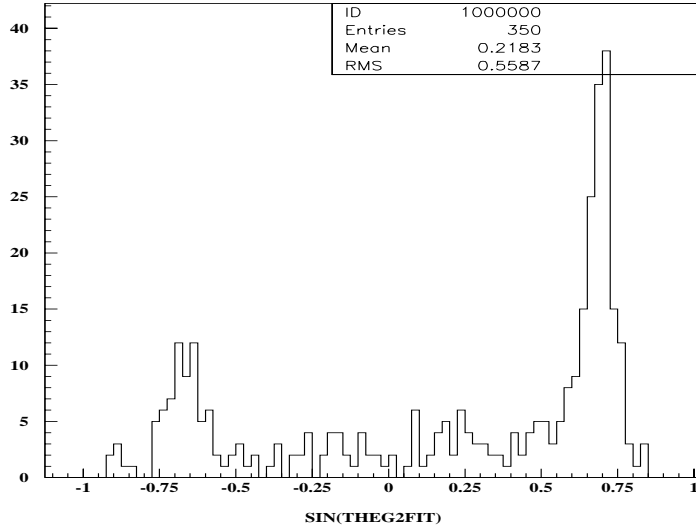
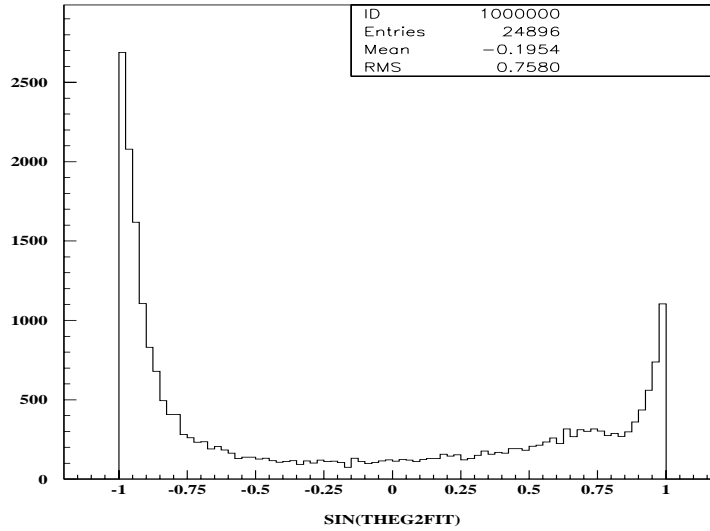


Figure 4.4: $\sin \theta_{fit}$ vs. $\sin \theta_{true}$

Figure 4.5: $\sin(\theta_{fit}), E_{fit} > 123\text{MeV}$ Figure 4.6: $\sin(\theta_{fit}), E_{fit} < 123\text{MeV}$

Cuts	Examined	Passed	Failed	Rejection
ECPV	289389	227038	62351	1.274628
RSPV	227038	197252	29786	1.151005
TGPV	197252	115190	82062	1.712406
ICPV	115190	112979	2211	1.019570
VCPV	112979	110311	2668	1.024186
COPV	110311	110033	278	1.002527
CMPV	110033	110013	20	1.000182
EUPV	110013	96443	13570	1.140705
PTOTAL	96443	95004	1439	1.015147
ETOTAL	95004	88295	6709	1.075984
RTOTAL	88295	88070	225	1.002555
PBPV	88070	78157	9913	1.1268344
TZMAX	78157	72016	6141	1.085273
WSTP	72016	67266	4750	1.070615
FIT	67266	67112	154	1.002295
PROB	67112	48282	18830	1.390000
BVPV	48282	25247	23035	1.912386

Table 4.5: Summary of Pass2 analysis

Chapter 5

Inefficiency

5.1 Single photon detection inefficiency

We have to know the total number of photons before online and offline photon vetoes to calculate the photon detection inefficiency. In E787, there are two K_{π_2} triggers called $K_{\pi_2}(1)$ and $K_{\pi_2}(2)$. $K_{\pi_2}(2)$ includes online photon vetoes, HEXCUT. $K_{\pi_2}(1)$ does not include it. To estimate the total number of the photons, we used $K_{\pi_2}(1)$ data. Then the tight π^+ selection cuts were applied. The kinematical fit was applied to the events for which one or more than one gammas were detected in BV. In this case the second photon was used for the fit if available. The number of the photons were counted by requiring $\text{Prob}(\chi^2) > 0.2$ (table.(5.3)).

The normalization factor was obtained by taking a ratio of 1 γ data to $K_{\pi_2}(1)$ data which passed the tight π^+ cut and the on-line 1 γ trigger conditions. The normalization factor was $609522/9675 = 63.00$ (See, table5.1,table5.2, where DETECTOR means all detector reconstructions, which are same as in Pass1(TRKTIM,UTCTRAK, RDTRAK,TARGET,ICOUNTER). PTOTAL,ETOTAL,RTOTAL and WSTP are the same definitions as in Pass2. BV bit requires at least 1 photon in BV at the online level, and BVHIT requires at least 1 photon in BV at the offline level.). This factor was multiplied to the numbers in the table 5.3.

Cuts	Examined	Passed	Failed	Rejection
DETECTOR	897809	835925	61884	1.074031
PTOTAL	835925	742407	93518	1.125966
ETOTAL	742407	672768	69639	1.103511
RTOTAL	672768	652183	20585	1.031563
BVHIT	652183	651932	251	1.000385
WSTP	651932	609522	42410	1.069579

Table 5.1: A cut summary for the normalization in 1 γ data

Cuts	Examined	Passed	Failed	Rejection
TRKTIM	713276	705628	7648	1.010839
UTCTRAK	705628	651386	54242	1.083272
RDTRAK	651386	643244	8142	1.012658
TARGET	643244	609523	33721	1.055324
ICOUNTER	609523	604903	4620	1.007638
PTOTAL	604903	291477	313426	2.075303
ETOTAL	291477	226382	65095	1.287545
RTOTAL	226382	206125	20257	1.098275
L1.1 bit	206125	135969	70156	1.515971
DC bit	135969	117298	18671	1.159176
IC bit	117298	117270	28	1.000239
WSTP	117270	106818	10452	1.097849
HEXCUT bit	106818	38737	60818	2.757519
BVHIT	38737	38468	269	1.006993
BV bit	38468	38306	162	1.004229
NG1 bit	38306	23369	14937	1.639180
\overline{EC} bit	23369	9675	13694	2.415401

Table 5.2: A cut summary for the normalization in $K_{\pi 2}(1)$ data

To compare the π^0 detection inefficiencies which are calculated in two ways, we changed the energy thresholds in BV. And we got four kinds of tables of missing photons (Table5.4-5.7).

Further, two correction factors were considered. First, the accidental loss in the photon vetoes was estimated by using $K_{\mu 2}$ data. After requiring the μ^+ , we applied all the photon vetoes and took the ratio of the number of remaining events before to after the vetoes. The correction factors were 0.7732, 0.7811, 0.7957 and 0.7993 when the energy threshold was 0.4, 1.0, 3.0 and 5.0 MeV, respectively. Second, the number of the events that a photon looked like two photons in BV was estimated by using $K_{\pi 2}$ events with $\pi^0 \rightarrow \gamma\nu$ decay in Monte Carlo simulation (UMC). After requiring the π^+ and applying all the photon vetoes except BV, we applied BV photon veto and took the ratio of the number of remaining events before to after the BV veto. (Note that the energy of a photon cluster was excluded prior to the veto.) The correction factors were 0.9084, 0.9404, 0.9836 and 0.9940 when the energy threshold was 0.4, 1.0, 3.0 and 5.0 MeV, respectively. The numbers in the tables5.4-5.7 were divided by both of the two correction factors. Then we got the inefficiency tables(Table5.8-5.11).

5.2 π^0 detection inefficiency

A π^0 detection inefficiency was estimated by using the single photon detection inefficiency tables and UMC. Since the energies and the directions of the photons from $\pi^0 \rightarrow \gamma\gamma$ were known in UMC, the probability to undetect both of the photons were calculated by the convolution method;

$$Inefficiency = \sum_{i=1}^N \frac{P(E_i^1, \theta_i^1)P(E_i^2, \theta_i^2)}{N} \quad (5.1)$$

where N is the number of events and P is the photon detection inefficiency.

The result is listed in the table(5.14). The errors were calculated as follows: First, we artificially fluctuated the photon detection inefficiency in each E- θ region assuming one standard deviation is equal to the statistical uncertainty, and made ten sets of the inefficiency tables. Then ten sets of pi0 detection inefficiencies were calculated by the convolution method. Finally, the standard deviation of the pi0 detection inefficiency was estimated from those ten values, and it was identified to be the error listed in table(5.14).

The π^0 detection inefficiency was also estimated by applying all the photon vetoes in $K_{\pi_2}(2)$ data(direct measurement). 1397701 $K_{\pi_2}(2)$ events were analyzed and 716563 events remained after π^+ cut. Applying all the photon vetoes, 0, 8, 53 and 89 events remained when the energy threshold in BV was 0.4, 1.0, 3.0 and 5.0 MeV, respectively. Cut summaries are listed in the table(5.12) and table(5.13), where cut definitions are same as in Pass1 and Pass2. PASS2PV means all the pass2 photon vetoes except BVPV and PBPV (that is, ECPV, RSPV, TGPV, ICPV, VCPV, COPV, CMPV and EUPV). Since the $K_{\pi_2}(2)$ data includes online photon veto, the normalization factor was multiplied to the number 716563. The factor was $106818/38737 = 2.76$, which was obtained by taking a ratio of the number of $K_{\pi_2}(1)$ events without HEXCUT to the number with it(see table5.2). And the accidental loss correction was considered. That is, the results were divided by the same correction factors (0.7732, 0.7811, 0.7957 and 0.7993 when the energy threshold was 0.4, 1.0, 3.0 and 5.0 MeV, respectively) as in the photon detection inefficiencies. Then the π^0 detection inefficiency(direct measurement) was obtained(Table5.14).

The inefficiency from $K_{\pi_2}(2)$ data becomes much larger as the threshold gets high. To find what happened, we analyzed UMC K_{π_2} data and got the similar results to real $K_{\pi_2}(2)$ data(table5.15).

We plotted the 'true' ϕ -difference of the two photons, and found that the event such that the two photons from the K_{π_2} decay hit the same segment of BV became dominant when the energy in BV was small. Figure(5.1) shows the way. The upper figure is the side view. The lower figure is the front view. Figure(5.2) shows the ϕ -difference when the energy in BV is greater than 5 MeV. Figure(5.3) is the one when the energy in BV is smaller than 5 MeV. The timing of a photon is determined by a mean of TDCs of both ends of a segment. So if the two photons hit the same segment, we misidentify the event that one photon hits BV with earlier timing than true timing. Such early photons will escape intime window and pass the veto.

To confirm this, we widened the time window to minus direction (from 'offset = 4.0 ns, window = 7.5 ns' to 'offset = 0.0, window = 11.5 ns') and analyzed the same UMC data. No event remained after all the photon vetoes although the energy threshold in BV was set to 5.0 MeV. That means the photons were tightly rejected even if the threshold was set to comparatively high. Also in the $K^+ \rightarrow \pi^+ \nu \bar{\nu}$ analysis, it will be useful to apply both the high-threshold-veto with wide-time-window and the low-threshold-veto with narrow-time-window.

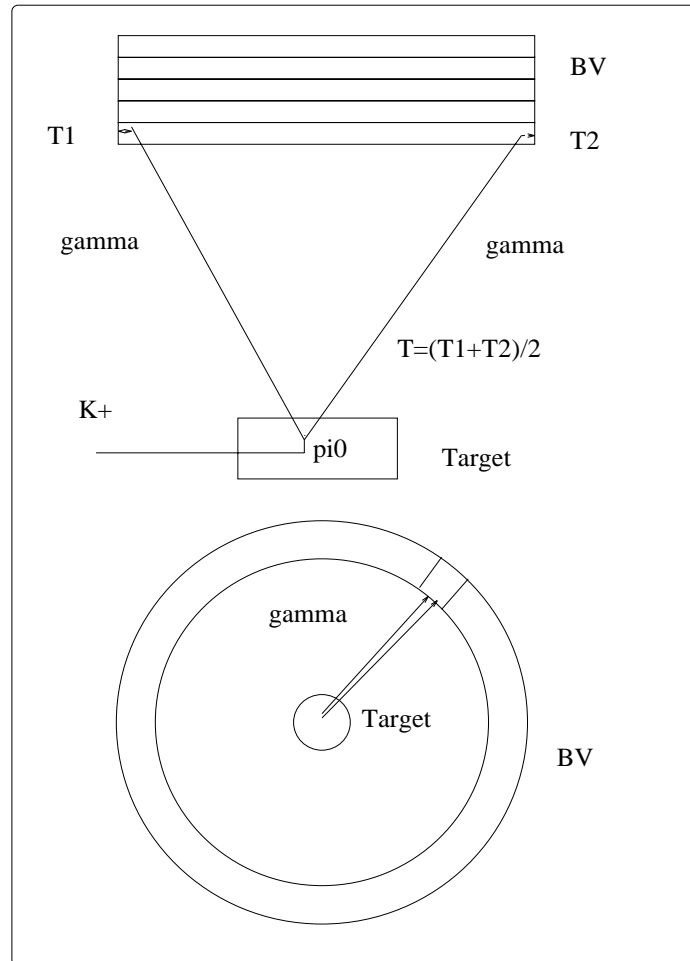


Figure 5.1: The way that the two photons hit the same segment.

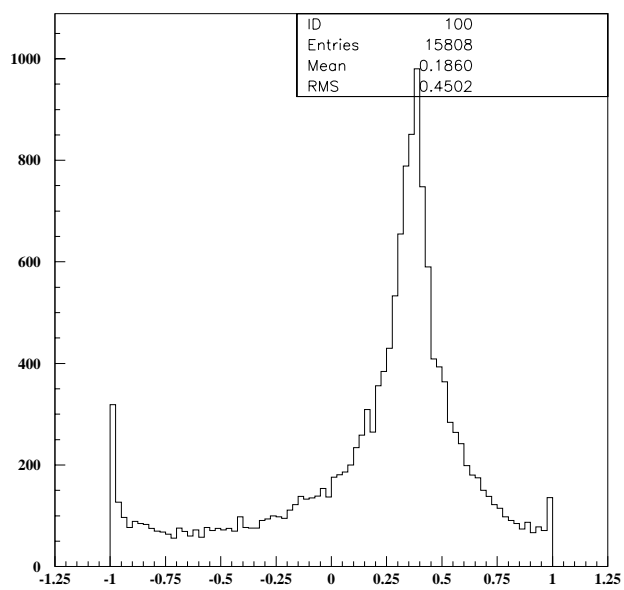


Figure 5.2: $\cos(\phi_{\gamma 1} - \phi_{\gamma 2})$ (E in BV > 5 MeV)

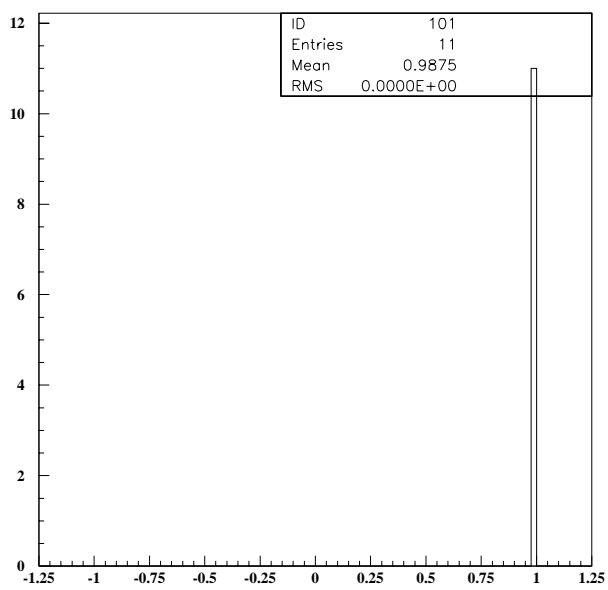


Figure 5.3: $\cos(\phi_{\gamma 1} - \phi_{\gamma 2})$ (E in BV < 5 MeV)

$\sin \theta = x$	$-1.0 < x < -0.8$	$-0.8 < x < -0.5$	$-0.5 < x < -0.2$	$-0.2 < x < +0.2$
$20 < E < 40$	1134	1247	1043	1399
$40 < E < 60$	1467	1335	1062	1228
$60 < E < 80$	899	1490	1169	1475
$80 < E < 100$	481	1560	1267	1571
$100 < E < 120$	208	1334	1252	1819
$120 < E < 140$	1235		1334	1916
$140 < E < 160$	856		1222	1771
$160 < E < 180$	431		1095	1740
$180 < E < 200$	142		980	1747
$200 < E < 225.5$	18		1207	2640

$\sin \theta = x$	$+0.2 < x < +0.5$	$+0.5 < x < +0.8$	$+0.8 < x < +1.0$
$20 < E < 40$	1037	1174	1038
$40 < E < 60$	956	1250	1373
$60 < E < 80$	1169	1464	938
$80 < E < 100$	1227	1478	533
$100 < E < 120$	1319	1327	256
$120 < E < 140$	1337	1236	
$140 < E < 160$	1359	886	
$160 < E < 180$	1256	580	
$180 < E < 200$	1096	229	
$200 < E < 225.5$	1453	26	

Table 5.3: The total number of photons in $K_{\pi_2}(1)$ data

$\sin \theta = x$	$-1.0 < x < -0.8$	$-0.8 < x < -0.5$	$-0.5 < x < -0.2$	$-0.2 < x < +0.2$
$20 < E < 40$	4217	1682	1038	1444
$40 < E < 60$	4116	503	177	222
$60 < E < 80$	1343	227	78	114
$80 < E < 100$	203	100	46	50
$100 < E < 120$	27	49	22	32
$120 < E < 140$	43		8	14
$140 < E < 160$	20		4	12
$160 < E < 180$	7		6	7
$180 < E < 200$	1		1	3
$200 < E < 225.5$	0		1	5

$\sin \theta = x$	$+0.2 < x < +0.5$	$+0.5 < x < +0.8$	$+0.8 < x < +1.0$
$20 < E < 40$	1407	1862	1922
$40 < E < 60$	317	677	1584
$60 < E < 80$	140	342	459
$80 < E < 100$	46	216	72
$100 < E < 120$	26	132	16
$120 < E < 140$	13	84	
$140 < E < 160$	9	61	
$160 < E < 180$	5	23	
$180 < E < 200$	4	5	
$200 < E < 225.5$	3	0	

Table 5.4: The number of missing photons ($E_{thres} = 0.4 MeV$)

$\sin \theta = x$	$-1.0 < x < -0.8$	$-0.8 < x < -0.5$	$-0.5 < x < -0.2$	$-0.2 < x < +0.2$
$20 < E < 40$	4418	1822	1150	1619
$40 < E < 60$	4325	537	199	251
$60 < E < 80$	1402	243	82	127
$80 < E < 100$	216	109	53	58
$100 < E < 120$	28	51	23	35
$120 < E < 140$	44		9	16
$140 < E < 160$	22		4	16
$160 < E < 180$	8		6	8
$180 < E < 200$	1		1	3
$200 < E < 225.5$	0		3	6

$\sin \theta = x$	$+0.2 < x < +0.5$	$+0.5 < x < +0.8$	$+0.8 < x < +1.0$
$20 < E < 40$	1521	1985	2010
$40 < E < 60$	345	717	1649
$60 < E < 80$	148	361	478
$80 < E < 100$	52	232	73
$100 < E < 120$	28	148	16
$120 < E < 140$	14	93	
$140 < E < 160$	10	66	
$160 < E < 180$	5	24	
$180 < E < 200$	6	5	
$200 < E < 225.5$	4	0	

Table 5.5: The number of missing photons ($E_{thres} = 1.0 MeV$)

$\sin \theta = x$	$-1.0 < x < -0.8$	$-0.8 < x < -0.5$	$-0.5 < x < -0.2$	$-0.2 < x < +0.2$
$20 < E < 40$	4948	2526	1922	2586
$40 < E < 60$	4690	702	357	398
$60 < E < 80$	1502	302	138	184
$80 < E < 100$	235	144	69	85
$100 < E < 120$	29	70	26	47
$120 < E < 140$	54		15	38
$140 < E < 160$	27		7	17
$160 < E < 180$	10		8	11
$180 < E < 200$	1		1	5
$200 < E < 225.5$	0		8	13

$\sin \theta = x$	$+0.2 < x < +0.5$	$+0.5 < x < +0.8$	$+0.8 < x < +1.0$
$20 < E < 40$	2181	2515	2213
$40 < E < 60$	493	878	1790
$60 < E < 80$	186	439	523
$80 < E < 100$	80	275	83
$100 < E < 120$	44	181	17
$120 < E < 140$	22	108	
$140 < E < 160$	13	78	
$160 < E < 180$	10	29	
$180 < E < 200$	9	7	
$200 < E < 225.5$	9	0	

Table 5.6: The number of missing photons ($E_{thres} = 3.0 MeV$)

$\sin \theta = x$	$-1.0 < x < -0.8$	$-0.8 < x < -0.5$	$-0.5 < x < -0.2$	$-0.2 < x < +0.2$
$20 < E < 40$	5410	3868	3604	4743
$40 < E < 60$	4830	839	570	678
$60 < E < 80$	1554	346	214	278
$80 < E < 100$	243	159	103	131
$100 < E < 120$	30	84	43	65
$120 < E < 140$	61		27	44
$140 < E < 160$	28		9	23
$160 < E < 180$	11		9	13
$180 < E < 200$	1		2	10
$200 < E < 225.5$	0		12	16

$\sin \theta = x$	$+0.2 < x < +0.5$	$+0.5 < x < +0.8$	$+0.8 < x < +1.0$
$20 < E < 40$	3446	3172	2422
$40 < E < 60$	654	992	1851
$60 < E < 80$	247	497	534
$80 < E < 100$	112	297	85
$100 < E < 120$	50	192	18
$120 < E < 140$	25	115	
$140 < E < 160$	16	83	
$160 < E < 180$	13	33	
$180 < E < 200$	13	7	
$200 < E < 225.5$	10	0	

Table 5.7: The number of missing photons ($E_{thres} = 5.0 MeV$)

$\sin \theta = x$	$-1.0 < x < -0.8$	$-0.8 < x < -0.5$	$-0.5 < x < -0.2$	$-0.2 < x < +0.2$
$20 < E < 40$	$8.5(\pm 0.28) \times 10^{-2}$	$3.1(\pm 0.12) \times 10^{-2}$	$2.2(\pm 0.10) \times 10^{-2}$	$2.4(\pm 0.09) \times 10^{-2}$
$40 < E < 60$	$6.3(\pm 0.19) \times 10^{-2}$	$8.6(\pm 0.45) \times 10^{-3}$	$3.7(\pm 0.31) \times 10^{-3}$	$4.1(\pm 0.30) \times 10^{-3}$
$60 < E < 80$	$3.4(\pm 0.15) \times 10^{-2}$	$3.4(\pm 0.25) \times 10^{-3}$	$1.5(\pm 0.18) \times 10^{-3}$	$1.7(\pm 0.17) \times 10^{-3}$
$80 < E < 100$	$9.5(\pm 0.80) \times 10^{-3}$	$1.5(\pm 0.15) \times 10^{-3}$	$8.2(\pm 1.3) \times 10^{-4}$	$7.2(\pm 1.0) \times 10^{-4}$
$100 < E < 120$	$2.9(\pm 0.60) \times 10^{-3}$	$8.3(\pm 1.2) \times 10^{-4}$	$4.0(\pm 0.86) \times 10^{-4}$	$4.0(\pm 0.71) \times 10^{-4}$
$120 < E < 140$	$7.9(\pm 0.12) \times 10^{-4}$		$1.4(\pm 0.48) \times 10^{-4}$	$1.6(\pm 0.43) \times 10^{-4}$
$140 < E < 160$	$5.2(\pm 1.2) \times 10^{-4}$		$7.4(\pm 3.7) \times 10^{-5}$	$1.5(\pm 0.45) \times 10^{-4}$
$160 < E < 180$	$3.6(\pm 1.4) \times 10^{-4}$		$1.3(\pm 0.50) \times 10^{-4}$	$9.1(\pm 3.4) \times 10^{-5}$
$180 < E < 200$	$1.6(\pm 1.6) \times 10^{-4}$		$2.4(\pm 2.4) \times 10^{-5}$	$3.9(\pm 2.2) \times 10^{-5}$
$200 < E < 225.5$	-		$1.9(\pm 1.9) \times 10^{-5}$	$4.3(\pm 1.9) \times 10^{-5}$
$\sin \theta = x$	$+0.2 < x < +0.5$	$+0.5 < x < +0.8$	$+0.8 < x < +1.0$	
$20 < E < 40$	$3.1(\pm 0.13) \times 10^{-2}$	$3.6(\pm 0.14) \times 10^{-2}$	$4.2(\pm 0.16) \times 10^{-2}$	
$40 < E < 60$	$7.5(\pm 0.48) \times 10^{-3}$	$1.2(\pm 0.06) \times 10^{-2}$	$2.6(\pm 0.10) \times 10^{-2}$	
$60 < E < 80$	$2.7(\pm 0.25) \times 10^{-3}$	$5.2(\pm 0.32) \times 10^{-3}$	$1.1(\pm 0.06) \times 10^{-2}$	
$80 < E < 100$	$8.5(\pm 1.3) \times 10^{-4}$	$3.3(\pm 0.25) \times 10^{-3}$	$3.1(\pm 0.39) \times 10^{-3}$	
$100 < E < 120$	$4.5(\pm 0.88) \times 10^{-4}$	$2.2(\pm 0.20) \times 10^{-3}$	$1.4(\pm 0.36) \times 10^{-3}$	
$120 < E < 140$	$2.2(\pm 0.61) \times 10^{-4}$	$1.5(\pm 0.17) \times 10^{-3}$		
$140 < E < 160$	$1.5(\pm 0.50) \times 10^{-4}$	$1.6(\pm 0.20) \times 10^{-3}$		
$160 < E < 180$	$9.0(\pm 4.1) \times 10^{-5}$	$9.0(\pm 1.9) \times 10^{-4}$		
$180 < E < 200$	$8.2(\pm 4.2) \times 10^{-5}$	$4.9(\pm 2.2) \times 10^{-4}$		
$200 < E < 225.5$	$4.7(\pm 2.7) \times 10^{-5}$	-		

Table 5.8: The inefficiency ($E_{thres} = 0.4 MeV$)

$\sin \theta = x$	$-1.0 < x < -0.8$	$-0.8 < x < -0.5$	$-0.5 < x < -0.2$	$-0.2 < x < +0.2$
$20 < E < 40$	$8.5(\pm 0.28) \times 10^{-2}$	$3.2(\pm 0.12) \times 10^{-2}$	$2.4(\pm 0.11) \times 10^{-2}$	$2.5(\pm 0.11) \times 10^{-2}$
$40 < E < 60$	$6.4(\pm 0.19) \times 10^{-2}$	$8.7(\pm 0.44) \times 10^{-3}$	$4.1(\pm 0.31) \times 10^{-3}$	$4.4(\pm 0.31) \times 10^{-3}$
$60 < E < 80$	$3.4(\pm 0.15) \times 10^{-2}$	$3.5(\pm 0.25) \times 10^{-3}$	$1.5(\pm 0.17) \times 10^{-3}$	$1.9(\pm 0.17) \times 10^{-3}$
$80 < E < 100$	$9.7(\pm 0.79) \times 10^{-3}$	$1.5(\pm 0.15) \times 10^{-3}$	$9.0(\pm 0.13) \times 10^{-4}$	$8.0(\pm 0.11) \times 10^{-4}$
$100 < E < 120$	$2.9(\pm 0.59) \times 10^{-3}$	$8.2(\pm 1.2) \times 10^{-4}$	$4.0(\pm 0.83) \times 10^{-4}$	$4.2(\pm 0.71) \times 10^{-4}$
$120 < E < 140$	$7.7(\pm 1.2) \times 10^{-4}$		$1.5(\pm 0.49) \times 10^{-4}$	$1.8(\pm 0.45) \times 10^{-4}$
$140 < E < 160$	$5.6(\pm 1.2) \times 10^{-4}$		$7.1(\pm 3.5) \times 10^{-5}$	$1.9(\pm 0.49) \times 10^{-4}$
$160 < E < 180$	$4.1(\pm 1.4) \times 10^{-4}$		$1.2(\pm 0.49) \times 10^{-4}$	$1.0(\pm 0.35) \times 10^{-4}$
$180 < E < 200$	$1.5(\pm 1.5) \times 10^{-4}$		$2.2(\pm 2.2) \times 10^{-5}$	$3.7(\pm 2.1) \times 10^{-5}$
$200 < E < 225.5$	-		$5.4(\pm 3.1) \times 10^{-5}$	$4.9(\pm 2.0) \times 10^{-5}$
$\sin \theta = x$	$+0.2 < x < +0.5$	$+0.5 < x < +0.8$	$+0.8 < x < +1.0$	
$20 < E < 40$	$3.2(\pm 0.13) \times 10^{-2}$	$3.6(\pm 0.14) \times 10^{-2}$	$4.2(\pm 0.16) \times 10^{-2}$	
$40 < E < 60$	$7.8(\pm 0.49) \times 10^{-3}$	$1.3(\pm 0.11) \times 10^{-2}$	$2.6(\pm 0.11) \times 10^{-2}$	
$60 < E < 80$	$2.8(\pm 0.24) \times 10^{-3}$	$5.4(\pm 0.31) \times 10^{-3}$	$1.1(\pm 0.11) \times 10^{-2}$	
$80 < E < 100$	$9.2(\pm 0.13) \times 10^{-4}$	$3.4(\pm 0.24) \times 10^{-3}$	$3.0(\pm 0.37) \times 10^{-3}$	
$100 < E < 120$	$4.6(\pm 0.88) \times 10^{-4}$	$2.4(\pm 0.21) \times 10^{-3}$	$1.4(\pm 0.35) \times 10^{-3}$	
$120 < E < 140$	$2.2(\pm 0.61) \times 10^{-4}$	$1.6(\pm 0.17) \times 10^{-3}$		
$140 < E < 160$	$1.6(\pm 0.50) \times 10^{-4}$	$1.6(\pm 0.20) \times 10^{-3}$		
$160 < E < 180$	$8.6(\pm 3.9) \times 10^{-5}$	$9.0(\pm 1.8) \times 10^{-4}$		
$180 < E < 200$	$1.2(\pm 0.48) \times 10^{-4}$	$4.7(\pm 2.1) \times 10^{-4}$		
$200 < E < 225.5$	$6.0(\pm 3.0) \times 10^{-5}$	-		

Table 5.9: The inefficiency ($E_{thres} = 1.0 MeV$)

$\sin \theta = x$	$-1.0 < x < -0.8$	$-0.8 < x < -0.5$	$-0.5 < x < -0.2$	$-0.2 < x < +0.2$
$20 < E < 40$	$8.9(\pm 0.29) \times 10^{-2}$	$4.1(\pm 0.14) \times 10^{-2}$	$3.7(\pm 0.14) \times 10^{-2}$	$3.7(\pm 0.13) \times 10^{-2}$
$40 < E < 60$	$6.5(\pm 0.19) \times 10^{-2}$	$1.1(\pm 0.05) \times 10^{-2}$	$6.8(\pm 0.42) \times 10^{-3}$	$6.5(\pm 0.37) \times 10^{-3}$
$60 < E < 80$	$3.4(\pm 0.14) \times 10^{-2}$	$4.1(\pm 0.26) \times 10^{-3}$	$2.4(\pm 0.21) \times 10^{-3}$	$2.6(\pm 0.19) \times 10^{-3}$
$80 < E < 100$	$1.0(\pm 0.08) \times 10^{-2}$	$1.9(\pm 0.16) \times 10^{-3}$	$1.1(\pm 0.14) \times 10^{-3}$	$1.1(\pm 0.12) \times 10^{-3}$
$100 < E < 120$	$2.8(\pm 0.56) \times 10^{-3}$	$1.1(\pm 0.13) \times 10^{-3}$	$4.2(\pm 0.83) \times 10^{-4}$	$5.2(\pm 0.77) \times 10^{-4}$
$120 < E < 140$	$8.9(\pm 1.3) \times 10^{-4}$		$2.2(\pm 0.59) \times 10^{-4}$	$4.1(\pm 0.66) \times 10^{-4}$
$140 < E < 160$	$6.4(\pm 1.3) \times 10^{-4}$		$1.2(\pm 0.44) \times 10^{-4}$	$1.9(\pm 0.47) \times 10^{-4}$
$160 < E < 180$	$4.7(\pm 1.5) \times 10^{-4}$		$1.5(\pm 0.52) \times 10^{-4}$	$1.3(\pm 0.39) \times 10^{-4}$
$180 < E < 200$	$1.4(\pm 1.4) \times 10^{-4}$		$2.0(\pm 2.0) \times 10^{-5}$	$5.8(\pm 2.6) \times 10^{-5}$
$200 < E < 225.5$	-		$1.4(\pm 0.48) \times 10^{-4}$	$1.0(\pm 0.28) \times 10^{-4}$
$\sin \theta = x$	$+0.2 < x < +0.5$	$+0.5 < x < +0.8$	$+0.8 < x < +1.0$	
$20 < E < 40$	$4.3(\pm 0.16) \times 10^{-2}$	$4.4(\pm 0.15) \times 10^{-2}$	$4.3(\pm 0.16) \times 10^{-2}$	
$40 < E < 60$	$1.0(\pm 0.06) \times 10^{-2}$	$1.4(\pm 0.06) \times 10^{-2}$	$2.7(\pm 0.10) \times 10^{-2}$	
$60 < E < 80$	$3.2(\pm 0.26) \times 10^{-3}$	$6.1(\pm 0.33) \times 10^{-3}$	$1.2(\pm 0.06) \times 10^{-2}$	
$80 < E < 100$	$1.3(\pm 0.15) \times 10^{-3}$	$3.7(\pm 0.25) \times 10^{-3}$	$3.2(\pm 0.37) \times 10^{-3}$	
$100 < E < 120$	$6.7(\pm 1.0) \times 10^{-4}$	$2.8(\pm 0.22) \times 10^{-3}$	$1.4(\pm 0.34) \times 10^{-3}$	
$120 < E < 140$	$3.3(\pm 0.72) \times 10^{-4}$	$1.8(\pm 0.18) \times 10^{-3}$		
$140 < E < 160$	$1.9(\pm 0.54) \times 10^{-4}$	$1.8(\pm 0.21) \times 10^{-3}$		
$160 < E < 180$	$1.6(\pm 0.51) \times 10^{-4}$	$1.0(\pm 0.19) \times 10^{-3}$		
$180 < E < 200$	$1.7(\pm 0.56) \times 10^{-4}$	$6.2(\pm 2.4) \times 10^{-4}$		
$200 < E < 225.5$	$1.3(\pm 0.42) \times 10^{-4}$	-		

Table 5.10: The inefficiency ($E_{thres} = 3.0 MeV$)

$\sin \theta = x$	$-1.0 < x < -0.8$	$-0.8 < x < -0.5$	$-0.5 < x < -0.2$	$-0.2 < x < +0.2$
$20 < E < 40$	$9.5(\pm 0.31) \times 10^{-2}$	$6.2(\pm 0.20) \times 10^{-2}$	$6.8(\pm 0.25) \times 10^{-2}$	$6.7(\pm 0.20) \times 10^{-2}$
$40 < E < 60$	$6.6(\pm 0.19) \times 10^{-2}$	$1.3(\pm 0.05) \times 10^{-2}$	$1.1(\pm 0.05) \times 10^{-2}$	$1.1(\pm 0.05) \times 10^{-2}$
$60 < E < 80$	$3.4(\pm 0.15) \times 10^{-2}$	$4.6(\pm 0.28) \times 10^{-3}$	$3.6(\pm 0.27) \times 10^{-3}$	$3.7(\pm 0.25) \times 10^{-3}$
$80 < E < 100$	$1.0(\pm 0.08) \times 10^{-2}$	$2.0(\pm 0.17) \times 10^{-3}$	$1.6(\pm 0.17) \times 10^{-3}$	$1.7(\pm 0.15) \times 10^{-3}$
$100 < E < 120$	$2.9(\pm 0.57) \times 10^{-3}$	$1.3(\pm 0.14) \times 10^{-3}$	$6.8(\pm 1.1) \times 10^{-4}$	$7.2(\pm 0.90) \times 10^{-4}$
$120 < E < 140$	$9.8(\pm 1.3) \times 10^{-4}$		$4.1(\pm 0.78) \times 10^{-4}$	$4.6(\pm 0.70) \times 10^{-4}$
$140 < E < 160$	$6.5(\pm 1.3) \times 10^{-4}$		$1.5(\pm 0.49) \times 10^{-4}$	$2.6(\pm 0.55) \times 10^{-4}$
$160 < E < 180$	$5.1(\pm 1.6) \times 10^{-4}$		$1.6(\pm 0.55) \times 10^{-4}$	$1.5(\pm 0.42) \times 10^{-4}$
$180 < E < 200$	$1.4(\pm 1.4) \times 10^{-4}$		$4.1(\pm 2.9) \times 10^{-5}$	$1.2(\pm 0.36) \times 10^{-4}$
$200 < E < 225.5$	-		$2.0(\pm 0.58) \times 10^{-4}$	$1.2(\pm 0.30) \times 10^{-4}$
$\sin \theta = x$	$+0.2 < x < +0.5$	$+0.5 < x < +0.8$	$+0.8 < x < +1.0$	
$20 < E < 40$	$6.6(\pm 0.24) \times 10^{-2}$	$5.4(\pm 0.18) \times 10^{-2}$	$4.7(\pm 0.17) \times 10^{-2}$	
$40 < E < 60$	$1.4(\pm 0.07) \times 10^{-2}$	$1.6(\pm 0.06) \times 10^{-2}$	$2.7(\pm 0.10) \times 10^{-2}$	
$60 < E < 80$	$4.2(\pm 0.30) \times 10^{-3}$	$6.7(\pm 0.35) \times 10^{-3}$	$1.2(\pm 0.06) \times 10^{-2}$	
$80 < E < 100$	$1.8(\pm 0.18) \times 10^{-3}$	$4.0(\pm 0.26) \times 10^{-3}$	$3.2(\pm 0.37) \times 10^{-3}$	
$100 < E < 120$	$7.6(\pm 1.1) \times 10^{-4}$	$2.9(\pm 0.22) \times 10^{-3}$	$1.4(\pm 0.34) \times 10^{-3}$	
$120 < E < 140$	$3.7(\pm 0.75) \times 10^{-4}$	$1.8(\pm 0.18) \times 10^{-3}$		
$140 < E < 160$	$2.4(\pm 0.59) \times 10^{-4}$	$1.9(\pm 0.21) \times 10^{-3}$		
$160 < E < 180$	$2.0(\pm 0.58) \times 10^{-4}$	$1.2(\pm 0.20) \times 10^{-3}$		
$180 < E < 200$	$2.4(\pm 0.66) \times 10^{-4}$	$6.1(\pm 2.4) \times 10^{-4}$		
$200 < E < 225.5$	$1.4(\pm 0.44) \times 10^{-4}$	-		

Table 5.11: The inefficiency ($E_{thres} = 5.0 MeV$)

Cuts	Examined	Passed	Failed	Rejection
TRKTIM	1397701	1383967	13734	1.009924
UTCTRAK	1383967	1345997	37970	1.028210
RDTRAK	1345997	1341015	4982	1.003715
TARGET	1341015	1296127	44888	1.034632
ICOUNTER	1296127	1290672	5455	1.004226
PTOTAL(pass1)	1290672	917313	373359	1.407014
RTOTAL(pass1)	917313	848888	68425	1.080605
1GAMMA	848888	838974	9914	1.011817
BVINTIME	838974	575996	262978	1.456562
ECINTIME	575996	214424	361572	2.686248
RSINTIME	214424	147078	67346	1.457893
ICINTIME	147078	135644	11434	1.084294
VCINTIME	135644	134097	1547	1.011536
PASS2PV	134097	55855	78242	2.400806
PTOTAL(pass2)	55855	55098	757	1.013739
ETOTAL	55098	52093	3005	1.057685
RTOTAL(pass2)	52093	51954	139	1.002675
WSTP	51954	48709	3245	1.066620
PBPV	48709	45373	3336	1.073524
BVPV(0.4MeV)	45373	0	45373	-
BVPV(1.0MeV)	45373	8	45365	5672
BVPV(3.0MeV)	45373	53	45320	856
BVPV(5.0MeV)	45373	89	45284	510

Table 5.12: A cut summary for direct measurement (numerator)

Cuts	Examined	Passed	Failed	Rejection
DETECTOR	1397701	1290672	107029	1.082925
PTOTAL(pass2)	1290672	882466	408206	1.462574
ETOTAL	882466	813106	69360	1.085303
RTOTAL(pass2)	813106	787034	26072	1.033127
WSTP	787034	716563	70471	1.098346

Table 5.13: A cut summary for direct measurement (denominator)

Energy threshold in BV (MeV)	inefficiency (convolution)	inefficiency (direct measurement)
0.4	$7.4 (\pm 1.1) \times 10^{-7}$	less than 1.3×10^{-6} (90% C.L.)
1.0	$9.0 (\pm 1.3) \times 10^{-7}$	$5.2 (\pm 1.8) \times 10^{-6}$
3.0	$1.8 (\pm 0.2) \times 10^{-6}$	$3.3 (\pm 0.5) \times 10^{-5}$
5.0	$2.9 (\pm 0.3) \times 10^{-6}$	$5.7 (\pm 0.6) \times 10^{-5}$

Table 5.14: π^0 detection inefficiency

Energy threshold in BV (MeV)	π^0 detection inefficiency
0.4	less than 1.6×10^{-5} (90% C.L.)
1.0	$1.6 (\pm 1.1) \times 10^{-5}$
3.0	$3.2 (\pm 1.6) \times 10^{-5}$
5.0	$8.7 (\pm 2.6) \times 10^{-5}$

Table 5.15: π^0 detection inefficiency (UMC, direct measurement)

Chapter 6

Barrel Veto Liner

We plan to install a new photon detector called Barrel Veto Liner (BVL) between RS and BV. If BVL is introduced, hi energy missing γ s are expected to decrease by the factor 0.37[5]. The inefficiencies in the table 5.8 were multiplied by the factor when the energies of missing photons were greater than 120 MeV. Then the π^0 detection inefficiency of $2.7(\pm 0.5) \times 10^{-7}$ was obtained. Furthermore, the asymmetry in figure 4.5 is expected to disappear after BVL is set. In the table 5.8, the inefficiencies in the region ' $+0.5 < \sin \theta < +0.8, 20 < E < 120$ ' and ' $+0.5 < \sin \theta < +1.0, 120 < E < 225.5$ ' were identified with ones in ' $-0.8 < \sin \theta < -0.5, 20 < E < 120$ ' and ' $-1.0 < \sin \theta < -0.5, 120 < E < 225.5$ ', respectively. Then the π^0 detection inefficiency of $2.3(\pm 0.3) \times 10^{-7}$ was obtained. That is, the BVL is expected to improve the π^0 detection inefficiency by the factor ~ 3 ($7.4 \times 10^{-7} / 2.3 \times 10^{-7}$).

Chapter 7

Conclusion

The single photon detection inefficiency as a function of energy and θ direction was measured using the special 1 γ data. It was around 10^{-2} in high energy regions, and around 10^{-5} in low energy regions.

From the table, the π^0 detection inefficiency was calculated by using a convolution method. It was 7.4×10^{-7} when the photon vetoes were tight.

A special π^0 missing mechanism was discovered. It can be removed easily by introducing a wide-time-window high-energy-threshold cut.

If Barrel Veto Liner is installed, the π^0 detection inefficiency will be reduced by the factor 3.

The branching ratio of $\pi^0 \rightarrow \nu\bar{\nu}$ will be lowered by the background subtraction with 14% errors.

Bibliography

- [1] BNL E787 collaborations. BNL, Princeton Univ., TRIUMF, KEK, INS-Tokyo and Osaka Univ.
- [2] T.Nakano,Y.Kuno E787 Technical Note No.256 (1993)
- [3] R.A.McPherson, PhD thesis (1995) Princeton Univ.
- [4] M.S.Atiya et al, Phys. Rev. Lett. **70**(1993) 2521
- [5] M.Kazumori, Master thesis (1997) Univ. of Tokyo
- [6] M.S.Atiya et al, Phys. Rev. Lett. **66**(1991) 2189

Acknowledgment

First, I greatly appreciate Dr. T.Nakano's many helpful suggestions and useful advises throughout my graduate course.

My special thanks are due to Prof. T.Kishimoto and Prof. Y.Nagashima.

I would like to express my great thanks to Dr. T.Shinkawa for giving me a lot of advises all the time not only during my stay in KEK.

I wish to express my gratitude to Dr. T.Komatsubara for telling me a lot of useful techniques in my study.

I would like to thank Prof. S.Sugimoto, Prof. T.Sato, Prof. Y.Yoshimura, Prof. S.Kabe, Prof. Y.Kuno, Prof. T.Inagaki, Prof. M.Kobayashi, Prof. M.Aoki, Dr. S.Kettell, Dr. S.Adler, Dr. M.Kuriki, Mr. N.Muramatsu, Mr. M.Kazumori, and all the members of E787 experiment.

I express my thanks to the members of Kishimoto laboratory and RCNP; Prof. T.Kishimoto, Dr. T.Nakano, Dr. H.Ohsumi, Dr. S.Ajimura, Dr. N.Kudomi, Dr. K.Kume, Mr. K.Hayashi, Mr. R.Hazama, Mr. K.Sugiyama, Mr. H.Miyawaki, Ms. H.Hayakawa, Mr. K.Morikubo, Mr. M.Komori, Mr. E.Saji, Mr. R.Sato, Mr. G.Kunitomi, Ms. S.Shiomi.